

Response of large area avalanche photodiodes to low energy x rays

T. R. Gentile, M. Bales, U. Arp, B. Dong, and R. Farrell

Citation: *Rev. Sci. Instrum.* **83**, 053105 (2012); doi: 10.1063/1.4714348

View online: <http://dx.doi.org/10.1063/1.4714348>

View Table of Contents: <http://rsi.aip.org/resource/1/RSINAK/v83/i5>

Published by the [American Institute of Physics](#).

Related Articles

Optical properties of armchair graphene nanoribbons embedded in hexagonal boron nitride lattices
J. Appl. Phys. **111**, 093512 (2012)

A normal incident quantum cascade detector enhanced by surface plasmons
Appl. Phys. Lett. **100**, 181104 (2012)

Two-color GaN/AlGaIn quantum cascade detector at short infrared wavelengths of 1 and 1.7 μ m
Appl. Phys. Lett. **100**, 181103 (2012)

Narrow-band long-/very-long wavelength two-color type-II InAs/GaSb superlattice photodetector by changing the bias polarity
Appl. Phys. Lett. **100**, 173511 (2012)

Photovoltaic infrared detection with p-type graded barrier heterostructures
J. Appl. Phys. **111**, 084505 (2012)

Additional information on Rev. Sci. Instrum.

Journal Homepage: <http://rsi.aip.org>

Journal Information: http://rsi.aip.org/about/about_the_journal

Top downloads: http://rsi.aip.org/features/most_downloaded

Information for Authors: <http://rsi.aip.org/authors>

ADVERTISEMENT



Special Topic Section:
PHYSICS OF CANCER

Why cancer? Why physics? [View Articles Now](#)

Response of large area avalanche photodiodes to low energy x rays

T. R. Gentile,¹ M. Bales,² U. Arp,³ B. Dong,⁴ and R. Farrell⁵

¹Stop 8461, National Institute of Standards and Technology, Gaithersburg, Maryland 20899, USA

²University of Michigan, Ann Arbor, Michigan 48104, USA

³Stop 8410, National Institute of Standards and Technology, Gaithersburg, Maryland 20899, USA

⁴Sotera Defense Solutions, Inc., Brookhaven National Laboratory, Upton, New York 11973, USA

⁵RMD Inc., Watertown, Massachusetts 02472, USA

(Received 23 January 2012; accepted 24 April 2012; published online 8 May 2012)

For an experiment to study neutron radiative beta-decay, we operated large area avalanche photodiodes (APDs) near liquid nitrogen temperature to detect x rays with energies between 0.2 keV and 20 keV. Whereas there are numerous reports of x ray spectrometry using APDs at energies above 1 keV, operation near liquid nitrogen temperature allowed us to reach a nominal threshold of 0.1 keV. However, due to the short penetration depth of x rays below 1 keV, the pulse height spectrum of the APD become complex. We studied the response using monochromatic x ray beams and employed phenomenological fits of the pulse height spectrum to model the measurement of a continuum spectrum from a synchrotron. In addition, the measured pulse height spectrum was modelled using a profile for the variation in efficiency of collection of photoelectrons with depth into the APD. The best results are obtained with the collection efficiency model. © 2012 American Institute of Physics. [<http://dx.doi.org/10.1063/1.4714348>]

I. INTRODUCTION

For an experiment to study neutron radiative beta-decay,¹⁻³ avalanche photodiodes (APDs) were employed to detect the visible light produced in scintillating crystals from the absorption of gamma rays with energies between 10 keV and 700 keV.⁴ More recently, the spectral range of the experiment has been extended by directly detecting 0.2 keV to 20 keV x rays with APDs.² Operation near liquid nitrogen temperature allowed us to obtain a nominal detection threshold of 0.1 keV, despite the large area of the APD employed. Although APDs have been used at energies above ≈ 1 keV (Refs. 5–8), we did not find reports of pulse height spectra at lower energies. To understand the response, we first employed x ray fluorescence using a 5.9 keV ⁵⁵Fe source,² but this only proved to be practical for energies at and above the aluminum K-shell line at 1.5 keV due to weak fluorescence yields and absorption of the emitted x ray by the fluorescing medium. Our next approach was to use synchrotron radiation from the Synchrotron Ultraviolet Radiation Facility (SURF III; Refs. 9 and 10) at the National Institute of Standards and Technology to observe the response to a continuum source with a well known spectrum. This facility had previously been used to calibrate the response of an APD X-ray spectrometer at energies as low as 700 eV.¹¹ The synchrotron results revealed that the pulse height spectra of the APD are complex, and that the detection efficiency is greatly decreased for energies below 1 keV. To understand this response, we performed measurements using monochromatic beams with energies between 350 eV and 1500 eV available at the U3C beam line at Brookhaven National Laboratory (BNL).^{12,13} We report the results of these measurements and application to modelling the APD response to continuum radiation. The modelling was tested with measurements on the BL3 beam line at SURF.

For the neutron radiative decay experiment, the APDs are operated in the bore of a 4.6 T superconducting magnet. Whereas APDs have previously been considered to be unaffected by magnetic fields,^{14,15} we recently reported that they are strongly affected at low temperatures when the magnetic field is in the plane of the APD.¹⁶ However, for the magnetic field normal to the plane of the APD, the effects were dramatically reduced. The studies discussed in this paper were performed in ambient magnetic fields.

We begin with a description of the APD apparatus in Sec. II. In Sec. III, we show results from our measurements with monochromatic beams of both the APD pulse height spectrum and detection efficiency. In Sec. IV, we discuss two models for the response: a phenomenological model based on a mathematical function that is fitted to the data and a model based on the collection efficiency of photoelectrons. Our results from SURF measurements are shown in Sec. V and application of the collection efficiency model to the SURF data is discussed in Sec. VI. We conclude the paper in Sec. VII.

II. APD APPARATUS

As shown in Fig. 1, the 28 mm by 28 mm APD (Ref. 17) was thermally sunk to the bottom of the inner reservoir of a Dewar.¹⁸ Although designed for use with liquid helium, both the inner and outer reservoirs of the Dewar were filled with liquid nitrogen. The APD was oriented at a 45° angle with respect to the BNL U3C and SURF BL3 beam lines because this orientation was relevant to our use in the neutron radiative decay experiment. The APD was secured with a G10 phenolic piece, with a cutout for the APD and apertures for the electrical connection pins. For the 1.3 mm thick APD, the depth of the cutout was slightly larger, 1.5 mm, to insure that the APD would not be stressed upon cooling.

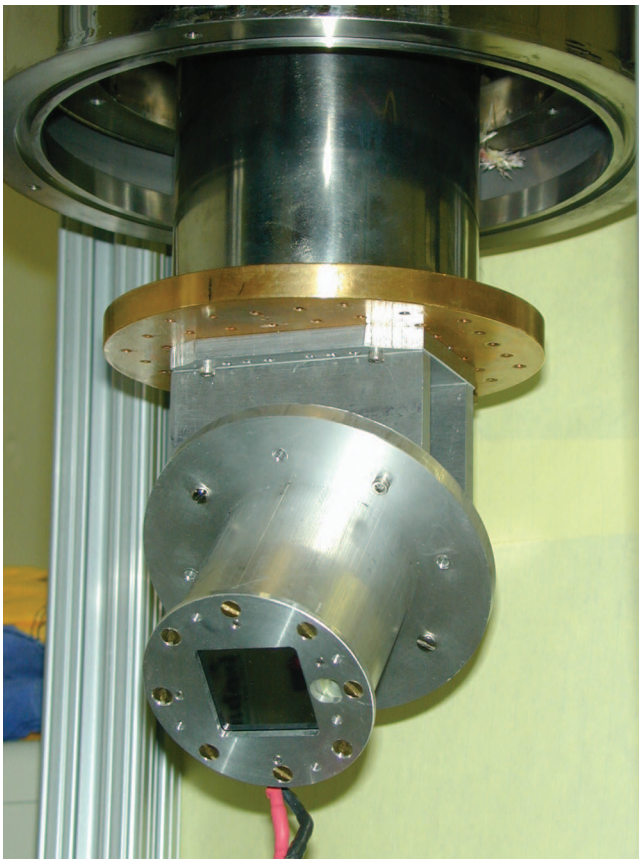


FIG. 1. Photograph of 28 mm by 28 mm APD (black square at bottom of photograph) mounted in the Dewar apparatus. The wiring for the APD, visible in the photograph, passes through an aperture in the aluminum cylinder behind the APD.

A 14 cm diameter, aluminum heat shield (not shown in photograph) attached to the annular outer reservoir extended 14 cm below the center of the APD. This shield had an 3.2 cm by 3.2 cm cutout for passage of x rays. The 16.5 cm diameter, room temperature, vacuum jacket extended 18 cm below the APD center and included a horizontal, 7 cm diameter, vacuum port for connection to the U3C or SURF beam lines. A 2.9 cm by 2.9 cm, 127 μm (0.005") thick polyimide window in the bottom endcap of the vacuum jacket allowed the APD to be illuminated with 5.9 keV x rays from an ^{55}Fe source, which provided a continuous calibration of the APD gain. This window was covered with aluminized Mylar and aluminum foil to block ambient visible light. The gain of APDs is sensitive to temperature;⁷ in this work, the gain was typically stable to $\approx 1\%$ once the Dewar apparatus was fully cooled. The temperature of the aluminum plate to which the APD was mounted was determined to be 94 K.

An oil-free turbomolecular pumping station was used to reduce the pressure in the chamber surrounding the APD to a typical base pressure of on the order of 10^{-6} mbar. To minimize the condensation of water vapor on the APD, the outer volume of the liquid helium Dewar was filled first. The pressure typically decreased to on the order of 10^{-7} mbar, then the inner volume was filled.

The APD signal was sent to a charge-sensitive preamplifier,¹⁹ followed by an amplifier set for a gain of 50

and a 3 μs shaping time constant. The output of the shaping amplifier was registered by a multichannel analyzer (MCA).²⁰ The lower level discriminator of the MCA was set to 0.9% of the total detected range of 10 keV, which was slightly below the noise wall. The APD was operated at a bias of 1330 V (≈ 50 V below breakdown).

III. MEASUREMENTS WITH MONOCHROMATIC X RAY BEAMS

A. APD pulse height spectra

The pulse height spectra of the APD were measured by illumination with x rays on the U3C beam line at BNL. Between the end of the U3C beam line and the connection to the Dewar, we had a large gate valve, bellows, electrically insulating nipple, and a small gate valve. To dramatically reduce the high flux available on U3C, a 15 μm diameter pinhole was located in the small gate valve 14 cm upstream of the APD. Energies above 1000 eV were obtained by using the second order of the beam line monochromator along with filters to extinguish the first order radiation. The counting rates were typically on the order of 1 kHz; saturation effects were not observed until the rate exceeded about 10 kHz. An aluminum/polyimide filter was also located in the small gate valve and could be inserted in the x ray beam to block any unwanted light but was not found to be necessary. Figure 2 shows the pulse height spectra of the APD for six energies between 350 eV and 1500 eV. Data were obtained for typical counting times of 100 s–200 s for a total of 17 energies: 350 eV–1000 eV in steps of 50 eV, and 1200 eV, 1300 eV, and 1500 eV. For the 1500 eV data, the small feature at 750 eV was due to first order x rays that were not completely removed for this case. In all our figures, data are shown without error bars for clarity. For both the BNL and SURF data, the total number of counts registered for a given configuration was on the order of 10^5 , hence the uncertainty from counting statistics in determining the overall shape of the spectrum was generally not significant.

B. Detection efficiency

To determine the absolute detection efficiency, we performed measurements of the count rate for a known x ray flux, where the flux was determined by calibrated photodiodes on the U3C beam line. For these measurements, the aforementioned pinhole was removed. The x ray flux was attenuated by apertures and/or slits available on the U3C beam line, which are located upstream of the calibrated photodiodes. For the small size apertures employed (1.5 mm maximum diameter), the entire x ray beam was incident on the APD. In some cases, the apertures were deliberately misaligned to reduce the flux. However, even at the lowest measurable photodiode current of on the order of 1 pA, the count rates at the APD were typically tens of kHz. To avoid saturation effects in the APD and allow for higher currents at the calibrated photodiode, we primarily used material filters to further attenuate the x ray intensity to obtain typical count rates of less than a few kHz from the APD. Typically, we directly determined the attenuation of

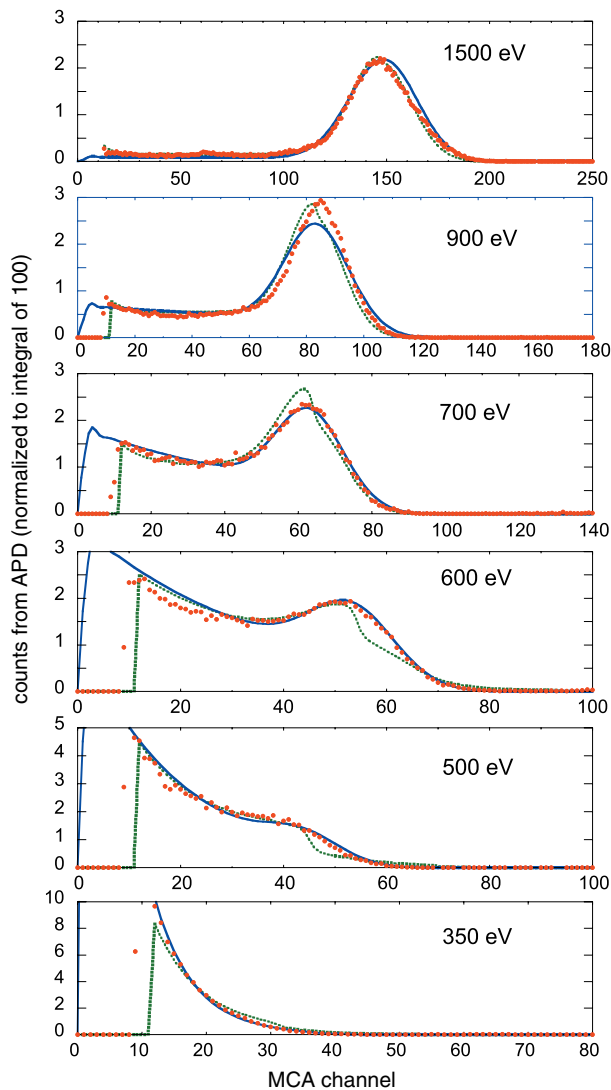


FIG. 2. Pulse height spectra from the APD for monochromatic x rays (BNL U3C) for six energies between 350 eV and 1500 eV (red filled circles). The x axis is in units of MCA channels, where the center of the response to the 5.9 keV line from an ^{55}Fe source was at channel 601. The background (response with x ray beam blocked), which consists primarily of a rapidly increasing noise wall below 120 eV (12 MCA channels) and a 4 Hz rate from the ^{55}Fe source, has already been subtracted. The background-subtracted data have been normalized to a total of 100 counts, integrated over the full detected energy range of 1000 MCA channels. The dotted, green curves show the fits to the phenomenological function discussed in Sec. IV A using the interpolated values for the fit parameters. The solid, blue curves shows the results of the collection efficiency model discussed in Sec. IV B.

these filters in separate measurements with larger apertures and/or open slits.

Figure 3 shows our measurements of the external efficiency, which is defined to be the number of counts registered above the detection threshold divided by the incident x ray flux. For reasons that were not understood, these measurements showed a dependence on the beam conditions, in particular different combinations of slit positions and aperture size. Uncertainties due to counting statistics and calibration of the U3C photodiodes were much smaller than the variations that were observed for different beam conditions. In addition, we checked the spatial uniformity of the APD with a ≈ 1 mm

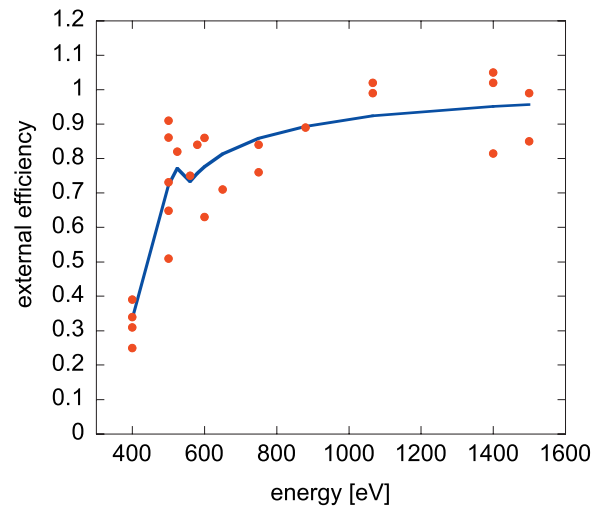


FIG. 3. External efficiency of the APD, which was determined as discussed in the text. The data were obtained from measurements with monochromatic x rays on the BNL U3C beam line. Error bars are not shown due to systematic issues discussed in the text. The solid, blue curve shows the efficiency that results from the product of the solid curve for the internal efficiency (see text) shown in Fig. 4 with the transmission of a 35 nm SiO_2 layer.

diameter beam of 750 eV x rays and found it to be better than 5%. Whereas the presence of this systematic was disappointing and not resolved in the beam time available, the measurements still indicate the expected efficiency of near unity at higher energies and a substantial decrease in efficiency below ≈ 500 eV. Some of this decrease is due to absorption by the doped glass deposited on the front of the APD, but the results in Fig. 2 show a large contribution from the response itself. This doped glass is dominantly SiO_2 , but there is significant doping in the glass layer and diffused into the front surface of the APD. Based on ellipsometry measurements, for which the glass layer was approximated to be pure SiO_2 , we determined an oxide thickness of (35 ± 10) nm. Figure 4 shows the efficiency corrected for x ray absorption in this layer, which we will refer to as the internal efficiency (IE). The behavior of the IE is consistent with the rapid degradation of the pulse height spectra below ≈ 500 eV. For the phenomenological modelling discussed in Sec. IV A, we employed the smooth curve shown (solid blue) to provide values for the IE at any energy. This curve is simply a smooth curve to match the data as well as possible. The curve in Fig. 3 shows the efficiency that results from the product of the IE curve and the transmission curve for the 35 nm SiO_2 layer. The dotted curve is based on the collection efficiency model discussed in Sec. IV B.

Accretion of frozen water vapor is a concern for a detector operated near liquid nitrogen temperature, and could lead to energy dependent absorption. However, at 200 eV (or at 525 eV, just above the K edge of oxygen), a thickness of 100 nm would be required to produce more than 15% absorption. Based on the absence of any time dependence in our measurements, as well as the internal consistency of our results, we believe that any possible effects from contamination are small.

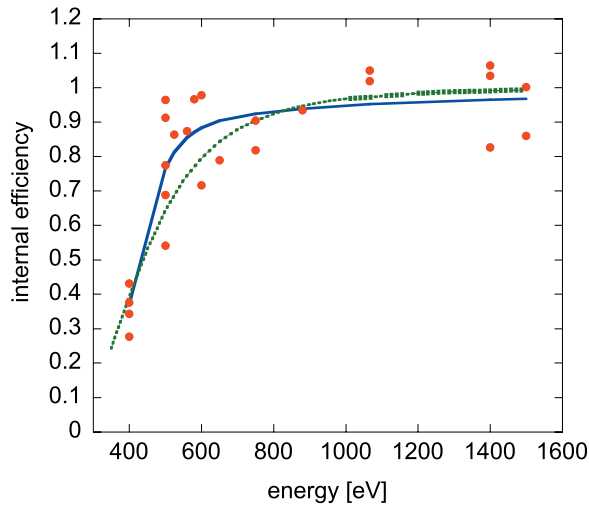


FIG. 4. Internal efficiency of the APD, which was determined as discussed in the text. The data were determined from measurements with monochromatic x rays on the BNL U3C beam line, corrected for x ray absorption in the glass layer on the APD. Error bars are not shown due to systematic issues discussed in the text. For the phenomenological modelling discussed in Sec. IV A, the solid, blue curve shown was employed to provide values for the internal efficiency at any energy. The dotted, green curve shows the internal efficiency determined from the collection efficiency model presented in Sec. IV B.

IV. MODELLING OF MONOCHROMATIC BEAM RESULTS

As the x ray energy is reduced below ≈ 1 keV, there is an increasing fraction of counts that have incomplete collection of photoelectrons, leading to a relatively flat response below the main peak. Below about 600 eV, very little of the response is in the main peak and an increasing fraction of the response exhibits low collection efficiency. Below 400 eV, the response is peaked below the noise wall. In Sec. IV A, we present a phenomenological function that fits the data. In Sec. IV B, we discuss the physical origin of these changes in the response and present a collection efficiency model that reproduces the data.

A. Phenomenological function

The response function, $R(A) = G(A) + F(A) + E(A)$, consists of a Gaussian peak $G(A)$, a flat component $F(A)$, and a zero-peaked, exponentially decreasing function $E(A)$ of the APD pulse amplitude A , where

$$G(A) = \frac{a_1}{a_3\sqrt{2\pi}} \exp\left(\frac{-(A - a_2)^2}{2a_3^2}\right), \quad (1)$$

$$F(A) = a_4(\pi/2 - \arctan(A - a_2)), \quad (2)$$

$$E(A) = a_5 \exp(-A/a_6). \quad (3)$$

The six fitting parameters are the Gaussian amplitude a_1 , the Gaussian width a_2 , the Gaussian center a_3 , the flat component's amplitude a_4 , the exponential amplitude a_5 , and the exponential width a_6 . The inverse tangent function allows for a flat level that decreases rapidly to zero for pulse amplitudes

above the Gaussian center. The fits can be improved by broadening the transition in the inverse tangent function, and allowing for the location of this transition to vary. However, the overall effect for modelling a broad continuum spectrum was not significant, and using the minimum number of parameters was useful for interpolation of these parameters between measurement energies. For the modelling of the SURF spectrum, we employed fits of the six parameters to interpolate these parameters between our 17 measured energies, thus yielding response functions for any energy. The functions for these interpolated parameters are shown in Fig. 2. For a given energy, better results are obtained for the best fit parameters for that energy rather than interpolated parameters. However, we show the results for the interpolated parameters in Fig. 2 because they are relevant to the application of the model to a continuum spectrum.

B. Collection efficiency model

Figure 5 shows the variation of the attenuation length in silicon with x ray energy. For energies below 1 keV and for the range between the Si K edge (1.84 keV) and about 2.5 keV, the attenuation length is less than $3 \mu\text{m}$. The efficiency for collection of photoelectrons is expected to be near zero at the front of the APD due to strong doping of the silicon. As the doping decreases rapidly in a distance of a micrometer or less, the collection efficiency increases. A slower decrease in doping occurs in the next $2 \mu\text{m}$ or $3 \mu\text{m}$, and some inefficiency might be expected within the $19 \mu\text{m}$ drift region. With these general ideas in mind, we experimented with calculating the expected pulse height spectra for monochromatic x rays from an assumed profile for the collection efficiency. We began with a simple linear profile in collection efficiency, similar to what has been reported to model the quantum efficiency of silicon photodiodes²¹ albeit for different physical effects. For each distance x , a collection efficiency $C(x)$ is assumed, and the distribution of pulse amplitudes $P(A)$ for a monochromatic x ray of energy E is calculated from

$$P(A) = \int P(x)G(A, x)dx, \quad (4)$$

where A is the amplitude of the pulse from the APD (units of eV), $P(x)$ is the probability of absorption of the x ray in the

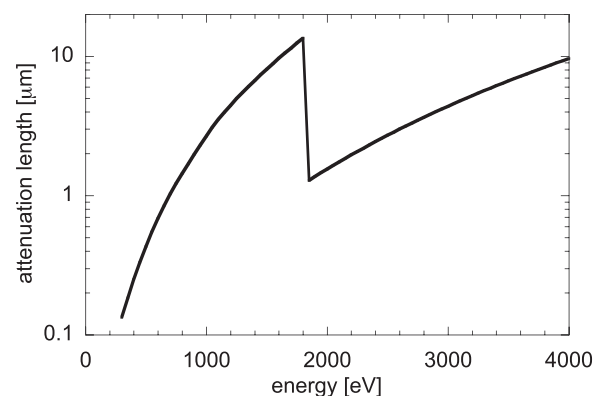


FIG. 5. Variation of the attenuation length in silicon with x ray energy. Data adapted from http://henke.lbl.gov/optical_constants.

distance interval x to $x+dx$, and $G(A,x)$ is the response for absorption at a given distance. $P(x) = \exp[-\alpha(E)x]\alpha(E)$, where $\alpha(E)$ is the absorption coefficient for an x ray of energy E . Accounting for the 45° tilt of the APD with respect to the x ray beam, the range of the integral was from zero to $60 \times 2^{1/2} \mu\text{m}$, where $60 \mu\text{m}$ is the distance to the end of the depletion region of the APD for normal incidence.

For a given energy E in eV, we assume a Gaussian function of the pulse amplitude and collection efficiency $C(x)$ given by

$$G(A, C) = \frac{1}{W(C)\sqrt{2\pi}} \exp\left(\frac{-(A - CE)^2}{2W^2(C)}\right), \quad (5)$$

where $W(C)$ is the width of the Gaussian. We assumed that the fractional width consists of an energy-independent component and a component that scales with the number of photoelectrons detected

$$\frac{W(C)}{E} = \frac{C}{2.345} \left[w_0^2 + \left(\frac{w_1}{\sqrt{CE}} \right)^2 \right]^{1/2}. \quad (6)$$

The parameters $w_0 = 0.12$ and $w_1 = 7.6 \text{ eV}^{1/2}$ were determined by fitting the energy dependence of the fractional full width at half maximum of the Gaussian components for the monochromatic beam data. The integral in Eq. (4) was performed numerically and the profile $C(x)$ was varied to visually match the experimental results for all 17 energies as well as possible. The profile is shown in Fig. 6 and the results of the model for this profile are shown for six energies in Fig. 2. To compare to the normalized data in Fig. 2, the model results were scaled by an IE that is determined from the model itself by evaluating the ratio of the response above the experimental threshold to the total response. The IE so determined is shown in Fig. 4. Note that this determination of the IE was not based on our efficiency measurements; it is entirely associated with the changes in the pulse height spectrum and a given experimental threshold. The results of this relatively simple collection efficiency model generally agrees with the

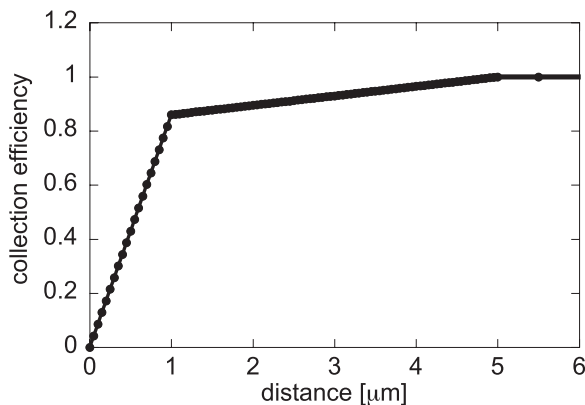


FIG. 6. Model for the variation of collection efficiency with distance into the APD. Since the x rays were incident on the APD at a 45° angle of incidence, the x axis values should be divided by $2^{1/2}$ for the actual penetration into the APD. The collection efficiency rises linearly from zero to 0.86 in $1.0 \mu\text{m}$, followed by a slower linear rise that reaches unity at $5.0 \mu\text{m}$ and stays at unity until the end of the depletion region at $60 \times 2^{1/2} \mu\text{m}$. The solid markers indicate the grid size for the model, which is $0.05 \mu\text{m}$ for the first $5 \mu\text{m}$, increases to $1 \mu\text{m}$ until a distance of $19 \mu\text{m}$, and finally $10 \mu\text{m}$ until the end.

data fairly well. It was found that a steep increase in the first micrometer of the APD was critical to obtain good agreement. Decreasing the endpoint of the slower slope from $5 \mu\text{m}$ to $\approx 3 \mu\text{m}$ or increasing it to $10 \mu\text{m}$ degraded the results. However, the details of this rise could be varied without much change in the agreement. Based on characteristics of the APD, we experimented with two different slopes, one between $1 \mu\text{m}$ and $3 \mu\text{m}$ followed by a slower slope from $3 \mu\text{m}$ to $10 \mu\text{m}$ or $20 \mu\text{m}$, but the results did not yield a noticeable improvement over a single slow rise.

V. MEASUREMENTS WITH SYNCHROTRON RADIATION

The BL3 beam line at the SURF III facility provided a known continuum spectrum for testing the models discussed in Sec. IV. Between the end of the BL3 beam line and the connection to the Dewar, we had a large gate valve, bellows, electrically insulating nipple, and a small gate valve. For the maximum available electron energy of $\approx 400 \text{ MeV}$, the x ray intensity in the regime of interest decreases steeply with increasing energy. In order to create spectra with most of the x ray intensity above the lower end of the usable range for the APD, filtering materials were added to the beam. A 2.00 mm aperture was installed in the small gate valve, which was located $\approx 14 \text{ cm}$ upstream of the APD. To block light, a $(0.120 \pm 0.012) \mu\text{m}$ aluminum filter supported by a nickel mesh was located next to the aperture. Figure 7 shows the results for three configurations, with increasing low energy content: for (a) and (b) the Al filter, a $(1.50 \pm 0.38) \mu\text{m}$ thick Al foil, and an aluminized Mylar sheet ($(6.350 \pm 0.25) \mu\text{m}$ Mylar, $(0.038 \pm 0.12) \mu\text{m}$ Al); for (c) and (d) the Al filter plus the $1.5 \mu\text{m}$ Al foil; and for (e) and (f) only the Al filter. The uncertainties quoted for these materials are based on manufacturers' tolerances. Data are shown for two electron beam energies, 380 MeV and 285 MeV . The SURF beam current was varied to yield typical count rates on the order of 1 kHz . These currents were (a) 10.2 nA , (b) $100 \mu\text{A}$, (c) 0.102 nA , (d), 0.106 nA , (e) 0.102 nA , and (f) 9.3 nA , where one electron in the ring yields 9.1 pA . The expected spectra were calculated from the product of the known SURF spectrum, the transmissions of the materials in the beam, and the aforementioned SiO_2 layer on the APD. The uncertainty in the SURF flux is typically less than 1% (Ref. 22) in the ultraviolet. However, it rises at higher energies due to the uncertainty of 5×10^{-4} in the SURF magnetic field,²³ reaching 2% at 1 keV and 5% at 4 keV .²⁴

Based on the manufacturer's data, an energy-independent transmission of 0.85 was included for the nickel mesh (70 lines per inch, $30 \mu\text{m}$ wide²⁵) in the Al filter. No correction was included for aluminum oxide layers on the filter and foils; these are expected to be $\approx 5 \text{ nm}$,²⁶ which would lead to less than 3% loss per layer for energies above 350 eV .

VI. APPLICATION OF MODELS TO SURF RESULTS

The primary goal of our studies is to confidently model the response of the APD to the neutron radiative decay

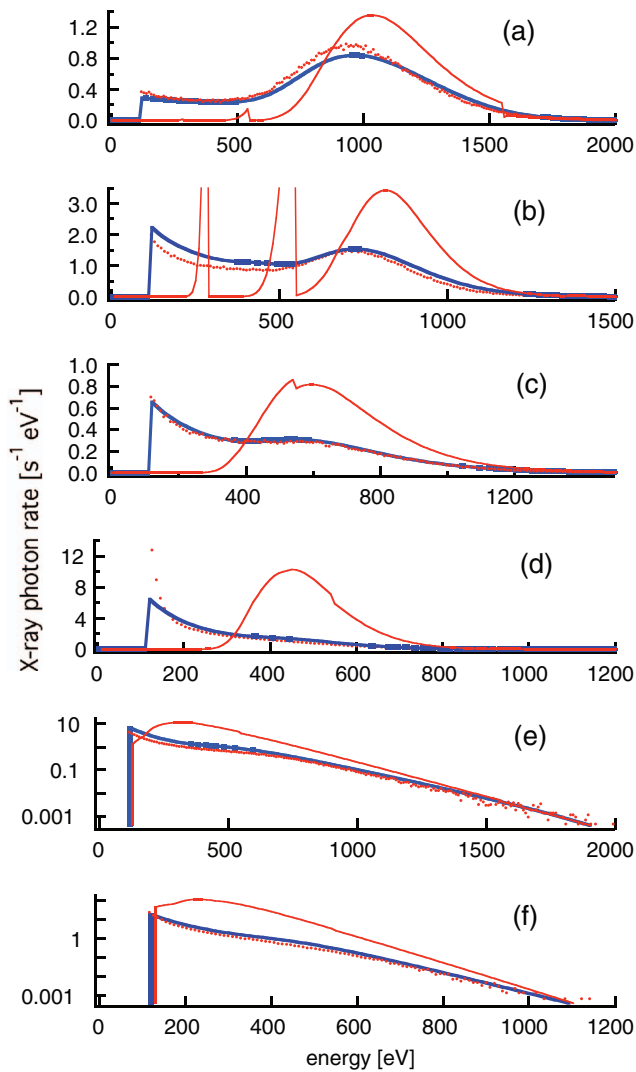


FIG. 7. Comparison of APD tests with synchrotron radiation (SURF BL3) to the results of the collection efficiency model (see Sec. IV B), performed with different materials in the x ray beam that are discussed in the text (see Sec. V). The materials are: for (a) and (b) the Al filter, Al foil, and aluminized Mylar sheet, for (c) and (d) the Al filter and Al foil, and for (e) and (f) only the Al filter. For (a), (c), and (e) the beam energy was 380 MeV, whereas for (b), (d), and (f) it was 285 MeV. The thin, red lines show the calculated spectra (incident on the APD, after the glass layer), the red markers show the measured response from the APD, and the thick blue line shows the results of convoluting the results of the collection efficiency model with the calculated spectra. For the calculated spectra, each plot shows the x ray photon rate in $s^{-1}eV^{-1}$ vs. x ray energy. For the APD response, the x axis was converted from MCA channel to energy using a calibration from an ^{55}Fe source.

spectrum. SURF provided a known continuum spectrum to test the modelling, and also allowed for tests of extrapolating the modelling outside of the region studied with monochromatic beams. Such extrapolation is possible because of the link between the x ray absorption depth and collection efficiency. In addition, results with continuum spectra allowed us to model APDs that were not tested at BNL, using a variation of the collection efficiency parameters. Hence, in this section we focus on application of the collection efficiency model (Sec. IV B) and do not show results for the phenomenological model (Sec. IV A). (Similar results were obtained with the phenomenological model but the collection

efficiency model yielded the best results and is more extendable.) Data were obtained with different filtering materials in the SURF beam to test the model for spectra with different characteristics.

A. SURF results with APD tested at BNL

Figure 7 shows the results of using the collection efficiency model to determine the expected response to the SURF spectra. For case (a) (aluminized Mylar, 380 MeV), the spectrum consists of a broad peak with energies between 700 eV and 1600 eV, and for case (b) (aluminized Mylar, 285 MeV), a peak with energies between 600 eV and 1200 eV, plus narrow spikes of transmission at ≈ 550 eV (oxygen K edge) and ≈ 280 eV (carbon K-edge). For case (c) (Al foil, 380 MeV), the spectrum consists of a peak with energies between 400 eV and 1200 eV, and for case (d) (Al foil, 285 MeV), a peak with energies between 350 eV and 800 eV. For these configurations, the x ray intensity in the Al transmission window between 20 eV and 75 eV is much higher than the higher energy peak: one order of magnitude for the 380 MeV data and three orders of magnitude for the 285 MeV data. However, as shown in the calculated spectra (incident on the APD, after the glass layer), these x rays should be completely absorbed by the doped glass layer on the APD.

For cases (e) and (f) (Al filter only), the intensity decreases by a few orders of magnitude between 300 eV and 1500 eV, hence these data are shown on a logarithmic scale for the count rate. Scatter due to counting statistics is apparent at high energies. The steep decrease in intensity with increasing energy leads to a substantial deviation of the measured response from the expected spectrum. The APD shows a decreasing response with decreasing energy, leading to an observed rate at the ≈ 300 eV peak that is an order of magnitude or more below the calculated spectrum.

In general, the modelling reproduces the data fairly well. If we make a small adjustment to the collection efficiency profile, we can closely match the data for cases (e) and (f) while still maintaining good agreement for the other cases. The small adjustment consists mainly of stretching the primary rise in collection efficiency over $1.3 \mu m$ instead of $1.0 \mu m$.

The uncertainties in the filtering material thicknesses affects the comparison of the convolution to the data. Since we did not have exact measurements for these values, we allowed for reasonable variations in the thickness values used in the calculations to best match the data. In the calculation of the convolution results shown in Fig. 7, the thickness of the $1.5 \mu m$ Al foil has been decreased to $1.02 \mu m$ to best match the data for all APDs tested at SURF. Since this value was slightly larger than the manufacturer's specified tolerance of $\pm 25\%$, we checked its transmission on the BNL X8A beam line¹² after the SURF experiments and modelling were completed. Based on measurements of the transmission of monochromatic x rays with energies between 1.0 keV and 2.1 keV, the actual thickness of the nominally $1.5 \mu m$ thick Al foil was determined to be $(0.93 \pm 0.12) \mu m$, consistent with our value. The aluminized Mylar thickness was decreased by

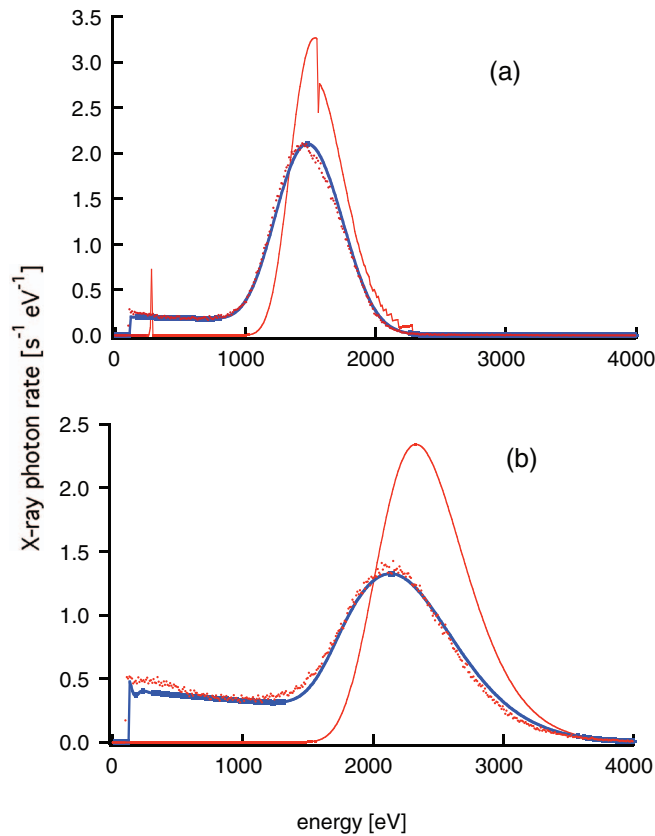


FIG. 8. APD tests with synchrotron radiation (SURF BL3), illustrating the change in response resulting from the change in attenuation length at the Si K edge. (a) SURF beam energy of 331 MeV, two layers of $25.4 \mu\text{m}$ ($0.001''$) polyimide before the APD, (b) 408 MeV, one layer of $127 \mu\text{m}$ ($0.005''$) polyimide. The thin, red lines show the calculated spectra (incident on the APD, after the glass layer), the red markers show the measured response of the APD, and the thick, blue line shows the results of convoluting the results of the collection efficiency model with the calculated spectra.

a factor of 0.96, which is within the manufacturer's specified tolerance.

The collection efficiency approach allows for modelling outside the range of energies that we studied with monochromatic beams. SURF was also employed to test the model for x rays with energies in the range near the Si K edge at 1.84 keV. Since the attenuation length just above the edge is comparable to that obtained at 800 eV, we expect the same distortion of the response. Using polyimide in the SURF x ray beam, we created broad peaks in the x ray spectrum incident on the APD, just below and above the K edge. (For these data an Al/polyimide filter ($0.15 \mu\text{m}$ Al, $0.20 \mu\text{m}$ polyimide) was employed rather than the $0.12 \mu\text{m}$ Al filter discussed in Sec. V.) Figure 8 shows the measured APD response for such spectra, along with the results of the collection efficiency model. The data show the expected increased distortion of the response for a spectrum just above the Si K edge as compared to just below the edge. The model agrees well with these data. Again the thickness of the polyimide was adjusted within tolerance to match the data; for the $25.4 \mu\text{m}$ ($0.001''$) polyimide the thickness was decreased by a factor of 0.92 and for the $127 \mu\text{m}$ ($0.005''$) polyimide the thickness was decreased by a factor of 0.96.

B. SURF results with other APDs

Whereas only one APD was studied at BNL, all three APDs used for the neutron radiative decay experiment were studied at SURF. Another APD from the same wafer yielded similar results, and could be modelled with minor changes in the collection efficiency profile. However, a third APD that was purchased later was found to yield much better low energy response but also some deviation from the expected proportionality between pulse height and x ray energy. Figure 9 shows the response of this APD for two cases: (a) 380 MeV, with only the Al/polyimide filter and (b) 408 MeV, one layer of $127 \mu\text{m}$ ($0.005''$) polyimide and the Al/polyimide filter, as for Fig. 8(b).

To model this APD, we replaced the product CE in Eq. (5) by $CEg(E)$, where $g(E)$ was fixed at 1.12 for $E \leq 2.5$ keV to match the data. To insure that $g = 1$ at the 5.9 keV energy of the x rays from the ^{55}Fe source used to calibrate the energy scale, we decreased g linearly to unity between $E = 2.5$ keV and $E = 5.9$ keV. The purpose of the parameter g is to modify the conversion of pulse height to an energy scale. The nature of this correction for nonlinearity is rather uncertain, so we chose the simplest approach to reproduce the data. Figure 9 shows the results for modelling the response of this APD with the collection efficiency profile shown in Fig. 10. The collection efficiency profile shown in Fig. 10 starts at a fairly high value of ≈ 0.4 , which implies that it rises to this value on a distance short compared to the $0.05 \mu\text{m}$ grid size for the modelling.

We expect that the improved low energy response of this APD is due to differences in the doping profile near the sensing surface. Regarding the nonlinearity, we speculated that it

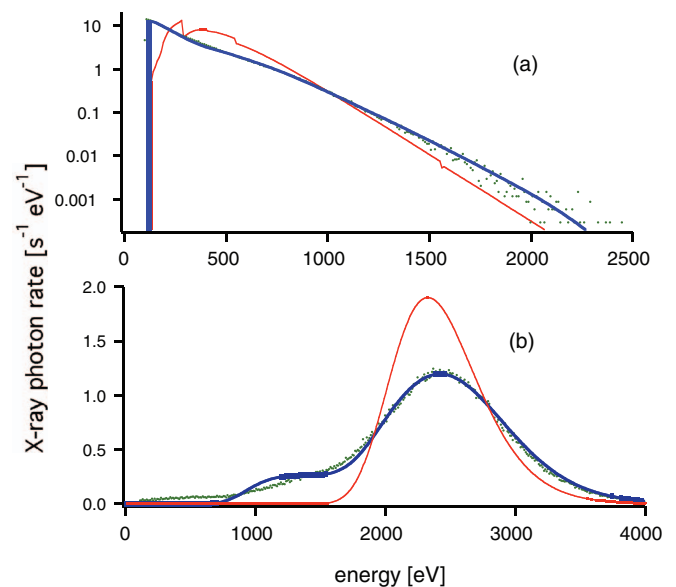


FIG. 9. Tests with synchrotron radiation (SURF BL3) for the APD discussed in Sec. VI B: (a) 380 MeV, with only the Al/polyimide filter and (b) 408 MeV, one layer of $127 \mu\text{m}$ ($0.005''$) polyimide and the Al/polyimide filter, as for Fig. 8(b). The thin, red lines show the calculated spectra (incident on the APD, after the glass layer), the red markers show the measured response of the APD, and the thick, blue line shows the results of convoluting the results of the collection efficiency model with the calculated spectra, for the profile shown in Fig. 10.

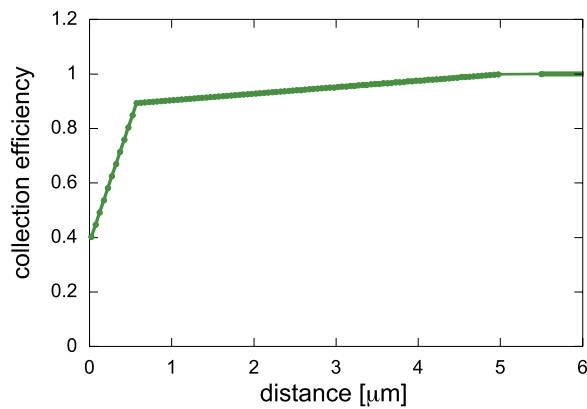


FIG. 10. Model for the variation of collection efficiency with distance into the APD, for the APD discussed in Sec. VI B. The collection efficiency rises linearly from 0.402 to 0.893 in 1.2 μm , followed by a slower linear rise that reaches unity at 5.0 μm and stays at unity until the end of the depletion region at $60 \times 2^{1/2} \mu\text{m}$.

could be due to the shorter n-type region in this device. The charge produced from the avalanche must travel to the electrodes through the undepleted portion of the region. Larger loss for a larger charge burst will lead to an energy-dependent gain. This speculation was supported by the observation of less nonlinearity at 20 V lower bias voltage.

Finally, we note that we used x ray fluorescence from CaSO_4 and aluminum, excited by the ^{55}Fe source, to produce peaks at 1.5, 2.3, 3.7, and 5.9 keV. For these experiments, the entire APD was illuminated and the counting rates are much lower than for the SURF results. We found that the nonlinearity observed for this APD using SURF was not clearly apparent for x ray fluorescence, which is not understood. Tests with rates as low as 25 Hz did not show any evidence for a rate dependence, but the difference in illuminated area could play a role.

VII. CONCLUSIONS

In conclusion, we have investigated detection of low energy x rays with a large area APD. We observed significant effects on the pulse height spectra for x ray energies below ≈ 1000 eV. These effects are rooted in the short attenuation length for such x rays coupled with reduced collection efficiency for photoelectrons produced in the first micrometer of the APD employed. The pulse height spectrum transitions from a simple Gaussian peak above ≈ 1000 eV to a zero-peaked, exponentially decreasing response below ≈ 500 eV. In the 500 eV–1000 eV range, the response is a Gaussian with a relatively flat background extending down to zero pulse amplitudes. This distortion of a simple Gaussian response is also evident in the range just above the Si K edge, and tests indicate that the collection efficiency model accurately reproduces experimental data. Despite this complex response, we were able to use both a phenomenological, mathematical model and a physical, collection efficiency model to reproduce the response to the continuous spectrum from synchrotron radiation. The collection efficiency model will be

employed for future analysis of the spectrum of neutron radiative decay.

ACKNOWLEDGMENTS

We thank P. Shaw, A. Farrell, and the entire SURF III staff for calculations of the SURF spectra and assistance with the measurements, K. Moy for assistance with the U3C measurements, Lee Richter for determination of the oxide layer thickness by ellipsometry, P. Shaw and M.S. Dewey for critical reading of the paper, and the entire neutron radiative decay collaboration for discussions. Use of the National Synchrotron Light Source, Brookhaven National Laboratory, was supported by the U.S. Department of Energy, Office of Science, Office of Basic Energy Sciences, under Contract No. DE-AC02-98CH10886.

- ¹R. L. Cooper, T. E. Chupp, M. S. Dewey, T. R. Gentile, H. P. Mumm, J. S. Nico, A. K. Thompson, B. M. Fisher, I. Kremisky, F. E. Wietfeldt, E. J. Beise, H. Breuer, K. G. Kiriluk, J. Byrne, K. J. Coakley, and C. Fu, *Phys. Rev C* **81**, 035503 (2010).
- ²R. L. Cooper, C. D. Bass, E. J. Beise, H. Breuer, J. Byrne, T. E. Chupp, K. J. Coakley, M. S. Dewey, B. M. Fisher, C. Fu, T. R. Gentile, M. McGonagle, H. P. Mumm, J. S. Nico, A. K. Thompson, and F. E. Wietfeldt, *Nucl. Instrum. Meth. A* **611**, 219 (2009).
- ³J. S. Nico, M. S. Dewey, T. R. Gentile, H. P. Mumm, A. K. Thompson, B. M. Fisher, I. Kremisky, F. E. Wietfeldt, T. E. Chupp, R. L. Cooper, E. J. Beise, K. G. Kiriluk, J. Byrne, and K. J. Coakley, *Nature (London)* **444**, 1059 (2006).
- ⁴T. R. Gentile, M. S. Dewey, H. P. Mumm, J. S. Nico, A. K. Thompson, T. E. Chupp, R. L. Cooper, B. M. Fisher, I. Kremisky, F. E. Wietfeldt, K. G. Kiriluk, and E. J. Beise, *Nucl. Instrum. Meth. A* **579**, 447 (2007).
- ⁵L. M. P. Fernandes, F. D. Amaro, A. Antognini, J. M. R. Cardoso, C. A. N. Conde, O. Huot, P. E. Knowles, F. Kottmann, J. A. M. Lopes, L. Ludhova, C. M. B. Monteiro, F. Mulhauser, R. Pohl, J. M. F. dos Santos, L. A. Schaller, D. Taqqu, and J. F. C. A. Veloso, *J. Inst.* **2**, P08005 (2007).
- ⁶L. Ludhova, F. D. Amaro, A. Antognini, F. Biraben, J. M. R. Cardoso, C. A. N. Conde, D. S. Covita, A. Dax, S. Dhawan, L. M. P. Fernandes, T. W. Hänsch, V.-W. Hughes, O. Huot, P. Indelicato, L. Julien, P. E. Knowles, F. Kottmann, J. A. M. Lopes, Y.-W. Liu, C. M. B. Monteiro, F. Mulhauser, F. Nez, R. Pohl, P. Rabinowitz, J. M. F. dos Santos, L. A. Schaller, D. Taqqu, and J. F. C. A. Veloso, *Nucl. Instrum. Meth. A* **540**, 169 (2005).
- ⁷M. Moszynski, M. Szawlowcki, M. Kapusta, and M. Balcerek, *Nucl. Instrum. Meth.* **485**, 504 (2002).
- ⁸R. Farrell, K. Vanderpuye, G. Entine, and M. R. Squillante, *IEEE Trans. Nucl. Science* **38**, 144 (1991).
- ⁹U. Arp, C. Clark, L. Deng, N. Faradzhev, A. Farrell, M. Furst, S. Grantham, E. Hagley, S. Hill, T. Lucatoro, P.-S. Shaw, C. Tarrío, and R. Vest, *Nucl. Instrum. Meth. A* **649**, 12 (2011).
- ¹⁰U. Arp, C. W. Clark, A. P. Farrell, E. Fein, M. L. Furst, and E. W. Hagley, *Rev. Sci. Instrum.* **73**, 1674 (2002).
- ¹¹S. M. Bailey, E. M. Rodgers, T. M. Garcia, K. Abnett, R. H. Ruhkuck, and J. Helmericks, in *Solar Physics and Space Weather Instrumentation*, edited by S. Fineschi and R. A. Viereck, Proc. SPIE **5901**, 590109 (2005).
- ¹²See <http://www.bnl.gov/u3cx8a> for information about the BNL U3C and X8A beam lines.
- ¹³R. J. Bartlett, W. J. Trela, F. D. Michaud, S. H. Southworth, R. W. Alkire, P. Roy, R. Rothe, P. J. Walsh, and N. Shinn, *Nucl. Instrum. Meth. A* **266**, 199 (1988).
- ¹⁴M. Boucher, O. Huot, P. E. Knowles, L. Ludhova, F. Mulhauser, L. A. Schaller, C. A. N. Conde, J. M. F. Dos Santos, L. M. P. Fernandes, J. F. C. A. Veloso, F. Kottmann, A. Antognini, R. Pohl, and D. Taqqu, *Nucl. Instrum. Meth.* **505**, 136 (2003).
- ¹⁵L. M. P. Fernandes, A. Antognini, M. Boucher, C. A. N. Conde, O. Huot, P. Knowles, F. Kottmann, L. Ludhova, F. Mulhauser, R. Pohl, L. A. Schaller, J. M. F. Dos Santos, D. Taqqu, and J. F. C. A. Veloso, *Nucl. Instrum. Meth.* **498**, 362 (2003).
- ¹⁶T. R. Gentile, C. D. Bass, J. S. Nico, H. Breuer, and R. Farrell, *Nucl. Instrum. Meth. A* **652**, 520 (2011).

- ¹⁷Model S2853, Radiation Monitoring Devices, Inc., Watertown, MA 02472. Certain trade names and company products are mentioned in the text or identified in an illustration in order to adequately specify the experimental procedure and equipment used. In no case does such identification imply recommendation or endorsement by the National Institute of Standards and Technology, nor does it imply that the products are necessarily the best available for the purpose.
- ¹⁸Model CNDT Research Dewar, Janis Research Company, 2 Jewel Drive, P.O. Box 696, Wilmington, MA 01887-0696.
- ¹⁹Model 2006, Canberra Industries, 800 Research Parkway, Meriden, Connecticut 06450.
- ²⁰Quantum MCA8000, Princeton Gamma-Tech, Inc., C/N 863, Princeton, NJ 08542-0863.
- ²¹T. R. Gentile, J. M. Houston, and C. L. Cromer, *Appl. Opt.* **35**, 4392 (1996), and references therein.
- ²²P.-S. Shaw, U. Arp, R. D. Saunders, D.-J. Shin, H. W. Yoon, C. E. Gibson, Z. Li, A. C. Parr, and K. R. Lykke, *Appl. Opt.* **46**, 25 (2007).
- ²³M. L. Furst, R. M. Graves, A. Hamilton, L. R. Hughey, R. P. Madden, R. E. Vest, W. S. Trezeciak, R. A. Bosch, L. Greenler, P. Robl, and D. Wahl, in *Proceedings of the 1999 Particle Accelerator Conference, New York, 1999*.
- ²⁴U. Arp, R. Friedman, M. L. Furst, S. Makar, and P.-S. Shaw, *Metrologia* **37**, 357 (2000).
- ²⁵H. Lopez, Luxel Corporation, Friday Harbor, WA 98250, private communication (2010).
- ²⁶E. Graper, Lebow Corporation, Goleta, CA, private communication (2010).